Passive Flow Modification Over the Supersonic and the Hypersonic Air-Intake System Using Bleed

Jayanta Sinha
Research Scholar
Amity Institute of Aerospace Engineering
Amity University Uttar Pradesh Noida
India

Sanjay Singh
Professor
Amity Institute of Aerospace Engineering
Amity University Uttar Pradesh Noida
India

Om Prakash
Professor
Department of Aerospace Engineering
University of Petroleum and Energy Studies
Dehradun
India

Dhruv Panchal
Postgraduate Student
Amity Institute of Aerospace Engineering
Amity University Uttar Pradesh Noida
India

The air intake should be operated at design conditions to achieve a high total pressure recovery and optimum mass capture ratio. The current research focuses on the numerical simulation of the supersonic and hypersonic air inlet and its starting and unstarting characteristics. 2D RANS equation for supersonic and hypersonic intake has been solved using the k-ωSST turbulence model. The in-house code and the algorithm based on the RANS equation have also been validated in due process and used for subsequent simulations. The sudden drop in mass capture ratio indicates the unstart condition of the intake. The presence of a bleed section has a commendable effect on the performance parameter of the air intake. A separation bubble was observed at the intake's entrance during the off-design conditions, resulting in performance losses. Four different bleed sections ranging in size from 1.6mm to 8.6mm were used, and simulations with bleed were run for different Mach numbers ranging from 3 to 8. The optimum bleed size of 3mm has been found quite effective in modifying Total pressure recovery within the optimum mass flow rate over the wide range of Mach numbers.

Keywords: *Hypersonic inlet, Pressure recovery, Mass capture ratio, shockwave, starting and unstarting of inlet, Bleed geometry, Total pressure ratio*

1. INTRODUCTION

Hypersonic inlet efficiency determines the overall engine performance. The performance of the hypersonic inlet is generally determined by two significant factors: total pressure recovery and mass capture ratio [1-4]. The inlet should provide better performance for its all-operating condition. Because of the high operating range of Mach numbers, the mixed compression type of inlet is the most convenient [5]. Flow field for the mixed compression type of inlet as shown in Figure 1.

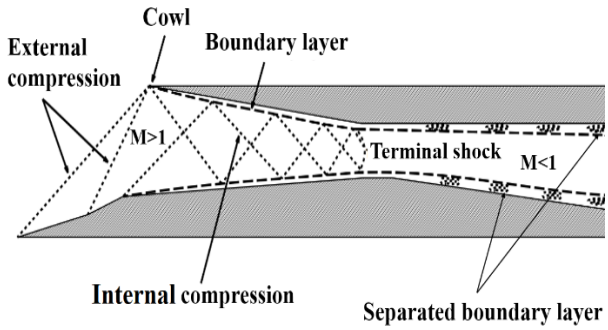

Figure 1. A mixed compression type of supersonic inlet [2]

Performance losses of intake affect the overall engine efficiency. Some of the causes of low inlet efficiency are flow spillage, different operating flight conditions, improper combustion, and multiple issues related to backpressure [6, 7].A high rate of spillage and discharging of shocks leads to a reduction in total pressure recovery and higher rates of flow distortion at the intake outlet [8,9]. Shockwave interaction with thin boundary layers increases the thickness of the local boundary layers at the region of internal compression, which is the prime cause of shock discharge, leading to an unstart [10, 11]. The prior solution to prevent the unstart condition is to provide the bleed flow section inside the intake [12]. The hypersonic flow contains high total temperature and enthalpy, which leads to structural complexity and cooling issues [13]. Predicting intake unstart reduces the occurrence, which is critical for hypersonic intake design. The researchers have performed numerical and experimental analyses to improve the unstart characteristics.

Reinartz et al. [14]reported the effect of different isolator geometry on overall inlet efficiency. Eight different isolator geometries of various lengths were tested experimentally to find that the increase in the isolator length reduces the pressure sensitivity of the intake. Schmitz and Bissinger [15] investigated two fixed geometry hypersonic inlets to find the starting and unstarting operations. To study the inlet starting characteristics, Yi Wang et al. [16]investigated and compared three inlet designs with varied internal contraction ratios.

Reinartz & Behr [17] performed extensive tests and analyses to improve a hypersonic intake's performance with sidewall compression, resulting in refinements in the MFR and starting characteristics. K. Raja Sekar et al. [18] investigated the two-dimensional rectangular

Received: February 2023, Accepted: May 2023
Correspondence to: Mr. Jayanta Sinha, Amity Institute of Aerospace Engineering, Amity University Uttar Pradesh, Sector 125, Noida, UP-201313, India
E-mail: jsinha1987@gmail.com
doi: 10.5937/fme2303329S

hypersonic mixed compression inlet at Mach 5. In their experiment, the throttling is simulated by inserting a wedge plug of variable heights at the exit of the isolator section and simulating different throttling ratios ranging from 0 to 0.7 in stages of 0.1. Lee et al. [19] provide much-needed insight into the boundary layer instability of the hypersonic cases and the experimental methods to detect them. These modes have also been accounted for in the current study. Unsteadiness in the hypersonic flow studied over the double wedge structure is of three types: vibration mode, oscillation mode, and pulsation mode [20]. Their separation depends on the separation zone's size and the shock wave's location. Janarthanam and Babu [21] carried out the 3D analysis of the mixed compression type of hypersonic inlet, and our selection of the turbulence model is largely based on this. To control the hypersonic boundary layer transition, active techniques like Plasma actuated flow control [22] and passive techniques like carbon fiber reinforced ceramic surfaces [23] have been utilized. Starting characteristics of hypersonic intake have been carried out by Barber et al. [24]. They studied starting characteristics and causes of unstarting related to the viscous effects and different turbulence models. A lot of motivation has been taken from this paper to develop the methodology for the CFD simulation of the present paper.

Many research papers have been published on air-intake optimization, and many have also used bleeds. Though most researchers have worked on buzz and other instabilities, only a few are there on the sizing and positioning of the bleed. It has also been found that limited work has been carried out on the effect of the bleed geometry on the supersonic and hypersonic flow modification. So a gap exists where none of the research could assert the exact bleed geometry and its location on the air intake for a range of Mach numbers ranging from supersonic to hypersonic, where it could provide optimum total pressure ratio and mass flow rate.

Moreover, the selection of bleed geometry depends on the intake design and the operating Mach. So, in this research paper, we have tried to bridge that gap, and through numerical analysis, we have provided the flow physics of the intake at start and unstart conditions at different Mach numbers.

This paper mainly focuses on the passive methods to improve their operating efficiency. The main application of this paper and the documented research work is that we have narrowed down the bleed geometry options, and we also identified the optimum dimension among them that can be used for both the Supersonic and the hypersonic flow regime with the help of bleed geometry.

The novelty of this paper lies in the fact that any high-speed air vehicle (like fighter jets) can operate over both flow regimes as per the mission profile, with minor modifications in the bleed geometry. With the advances in research in Ramjet and Scramjet propulsion systems, this kind of study provides great insight into developing the air-intake system of fighter jets, guided missiles, or other high-speed air-breathing engines.

We have modified the intake geometry given by Emami and Trexlar [25]. We simulated the same air-intake model, firstly, without bleed and then with the bleed, to obtain the modification in the optimum performance parameter as the function of the bleed geometry. The unique contribution of this research is that it presents the internal flow physics, performance parameter characteristics, and optimum bleed geometry selection over a wide range of Mach numbers ranging from 2.5 to 8.It forms the basis of further research and in-house code development to evaluate the different back pressure dynamics.

The sole purpose of this paper is to obtain the effect of bleed on a particular intake and then optimize the bleed size for the given intake geometry. Over fifty bleed sizes have been analyzed, after which a set of 4 slotted bleeds have been considered in the present research paper. Unsteady phenomena and buzz have yet to be covered in this paper as it will make this paper extremely lengthy.

2. GEOMETRY AND GRID

The geometry of the inlet used for experimental inves–tigation by Emami and Trexler [25] is shown in Figure 2. The geometry has a mixed compression type of inlet with one compression ramp. The bleed case's geometry has been modified (see Fig. 3).

The four different bleed cases have been chosen as 1.3mm, 3mm, 7.1mm, and 8.6mm. The length of the model is 338 mm.

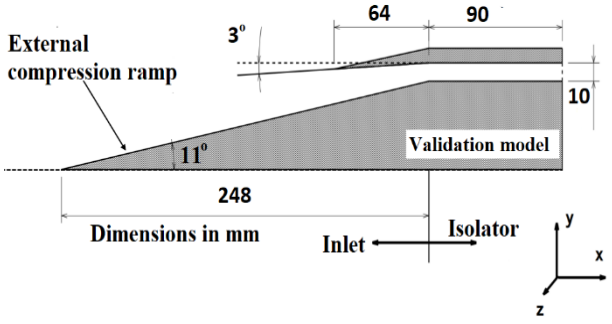

Figure 2. Air intake geometry of Emami and Trexler [25] for which the validations are carried out

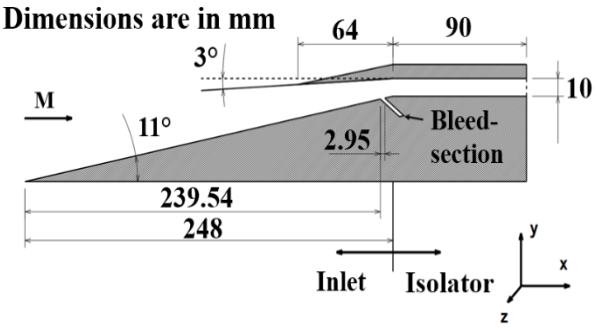

Figure 3. Modified Air inlet geometry with bleed

The inlet geometry is the symmetry of the mid-plane, so according to that, the computational domain has been created (see Fig 4) and simulated. The computational domain (with bleed) and the named selection are shown in Figure 4.

Different grid systems for the fluid domain have been developed to capture the shockwave structure. Figure 5 depicts the grid system for the entire comput–ational domain and an enlarged view of the system

chosen for the isolator. The height of the far field from the base is two times the length of the upstream sym–metry line of length 'L'. The Span of the computational domain is also 2L. Such a square computational domain provides better control of the grid generation.

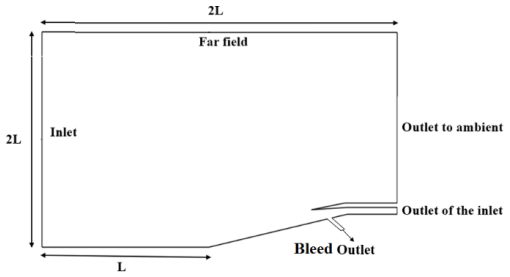

Figure 4. Named selections for the simulation

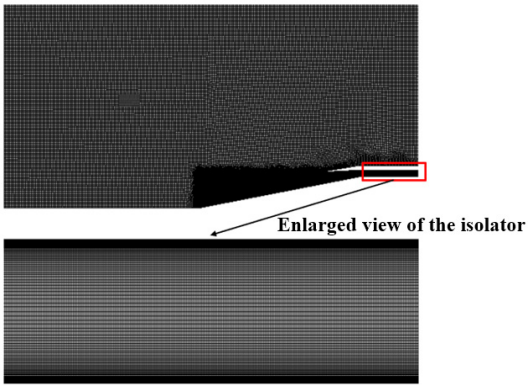

Figure 5. Grid system

The grid system is selected after extensive grid refinement exercises (see Fig. 6). We chose a fine mesh over a superfine mesh to reduce the computational time for the parametric studies. Figure 7 compares the lower ramp wall pressure variation for experimental [25] and computational reference data [2]. A number of cells rounded off to the order of 10^5 in different mesh types are shown in Table 1.

Table 1. Grid Types for grid independence study

Mesh types	No. of cells (Rounded off to nearest lacs)
Coarse	200000
Medium	300000
Fine	400000
Superfine	500000

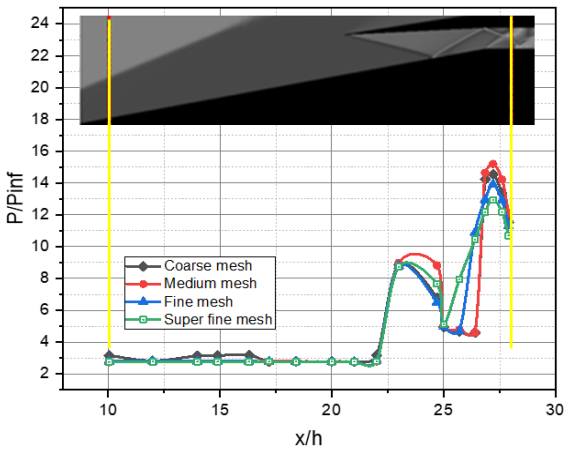

Figure 6. Grid independence check

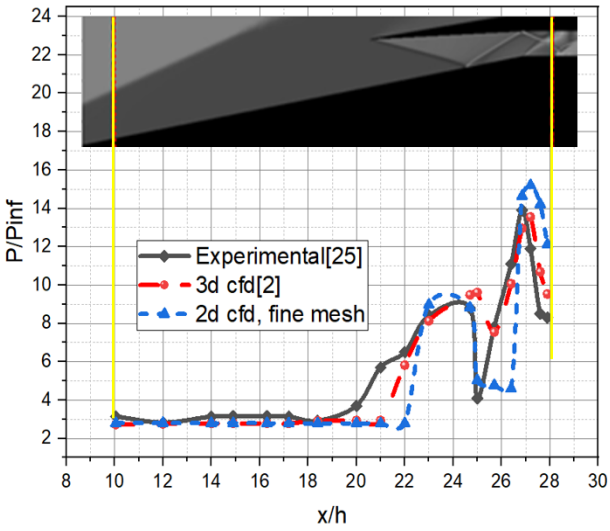

Figure 7. Numerical validation check with reference data [2] & [25]

The simulation was performed based on the data reported by Saha et al.[2], and different Mach numbers have been imposed by varying the total pressure. Two air outlets were created, one for the inlet and another for the ambient outlet. To implement the bleed, an additional outlet was created (Fig.4). In the current solution; the simulations were performed in a steady-state, density-based implicit Reynolds-averaged Navier-Stokes equa–tions (RANS) solver with a K-ω SST turbulence model. 2nd order spatially accurate roe-flux difference splitting scheme for spatial discretization and a 2nd order implicit Euler Scheme for temporal discretization have been used. The solver is verified using benchmark data generated from a closed-form analytical model [26-27]. Further–more, numerical results are validated using the experimental data given by Emami and Trexlar [25] and computational data given by Saha and Chakraborty [2].

Since no experimental work has been undertaken supporting the present research work, we have validated the work using the published paper by Milicev [28] and Damljanović et al. [29]. The off-design performance of the model in the wind tunnel has been studied based on the work of Damljanović et al. [30].

Table 2. Solver set-up

Scheme/parameters	Type/quantities
Solver precision	Double precision
Solver type	Density-based implicit, steady state
RANS	k-ω SST (2 PDE model)
Inviscid flux scheme	Roe flux-difference splitting scheme
Spatial discretization	Second-order upwind scheme
Gradient evaluation	Least squares cell-based

3. GOVERNING EQUATIONS

For the present simulation, the k-ω shear stress model has been used. ‘k' represents the turbulent kinetic energy, and 'ω’ represents the specific dissipation rate.

Turbulence viscosity is obtained as a function of both ‘k’ and ‘ω’.

$$\mu_t = \frac{(\rho \alpha k)}{\omega} \tag{1}$$

Turbulent kinetic energy (k) equation:

$$\frac{\partial}{\partial t}(\rho k) + \frac{\partial}{\partial x_i}(\rho k u_i) = \frac{\partial}{\partial x_j}\left[\left(\frac{\mu + \mu_t}{pr_k}\right)\left(\frac{\partial k}{\partial x_j}\right)\right] + \tag{2}$$

$$+G_k - \rho e$$

Specific dissipation rate (ω) equation:

$$\frac{\partial}{\partial t}(\rho \omega) + \frac{\partial}{\partial x_i}(\rho \omega u_i) = \frac{\partial}{\partial x_j}\left[\left(\frac{\mu + \mu_t}{pr_\omega}\right)\left(\frac{\partial \omega}{\partial x_j}\right)\right] - \beta^* \rho \omega^2 \tag{3}$$

The governing equation system that regulates the turbulent compressible gas is as follows:

Continuity equation:

$$\frac{\partial p}{\partial t} + \frac{\partial}{\partial x_i}(\rho u_i) = 0 \tag{4}$$

Momentum equation:

$$\frac{\partial}{\partial t}(\rho u_i) + \frac{\partial}{\partial x_i}(u_i u_j) + \frac{\partial p}{\partial x_i} = \frac{\partial \tau_{ij}}{\partial x_j} \tag{5}$$

Energy equation:

$$\frac{\partial}{\partial t}(\rho E) + \frac{\partial}{\partial x_i}(\rho u_i E) = \frac{\partial}{\partial x_j}\left[\left(\gamma + \frac{\gamma_t}{Pr_\gamma}\right)\frac{\partial T}{\partial x_j}\right] + Q \tag{6}$$

The term "turbulent shear stress" refers to the amount of force exerted by a moving object. It is expressed as:

$$\tau_{ij} = \mu\left(\frac{\partial u_i}{\partial x_j}\right) + \left(\frac{\partial u_j}{\partial x_i}\right) \tag{7}$$

$\mu = \mu_t + \mu_l$, is the total viscosity;

μ_l, μ_t being the laminar and turbulent viscosity, respectively.

Laminar viscosity calculated from Sutherland law as

$$\mu_1 = \mu_{ref}\left(\frac{\partial T}{\partial T_{ref}}\right)^{\frac{3}{2}}\left(\frac{T_{ref} + S}{T + S}\right) \tag{8}$$

The stress tensor is expressed as a turbulent viscosity (μ_t) function in eddy viscosity models. Based on dimensional analysis, a few variables (k, ε, ω) are designated as follows:

Turbulent kinetic energy k,

$$k = \overline{u_i u_i} / 2 \tag{9}$$

Turbulent dissipation rate ε,

$$\varepsilon = \overline{\frac{\partial u_i'}{\partial x_j}\left[\frac{\partial u_i'}{\partial x_j} + \frac{\partial u_j'}{\partial x_i}\right]} \tag{10}$$

Specific dissipation rate ω

$$\omega = \frac{\varepsilon}{k} \tag{11}$$

The turbulent viscosity u_t is denoted by

$$\mu_t = c_\mu\left(\frac{\rho k^2}{\varepsilon}\right) \tag{12}$$

The heat flux is calculated as,

$$q = -\gamma \frac{\partial T}{\partial x_i} \tag{13}$$

4. NUMERICAL VALIDATION STUDY

4.1 Surface pressure distribution

The wall Pressure distribution across a lower ramp compared with the experimental work done by Emami and Trexler [25] and the 3D computational work done by Saha and Chakraborty [2], as shown in Figure 7. The pressure and distance are shown in non-dimensional terms. In the P/Pinf, Pinf is the free stream pressure, and in x/h, h is the intake throat height. The results show differences near the cowl shock impingement point, and overall good agreements are demonstrated with the experimental. However, certain variation at x/h =26 and x/h=28 can be attributed to the fact that this is a 2D simulation, whereas the others are experimental and the 3D simulation. Still, we have managed to obtain a good match with both the papers when we consider the Total pressure ratio and the Mass capture ratio.

4.2 Mass capture ratio & total pressure recovery

The inlet should perform optimally in all operating conditions. The mass capture ratio (MCR) and total pressure ratio (TPR) are essential factors in the overall efficiency of the inlet [1,2]. Figure 8 compares the mass capture ratio (MCR) for various free-stream Mach numbers. The findings are compared with the same set of reference data [2, 25]. From the graph, figure 8, we can observe that as the Mach number increases, the MCR also increases, indicating low spillage for higher values of Mach numbers (4 < M < 8). A good estimation of the numerical data can be seen here with the experimental data.

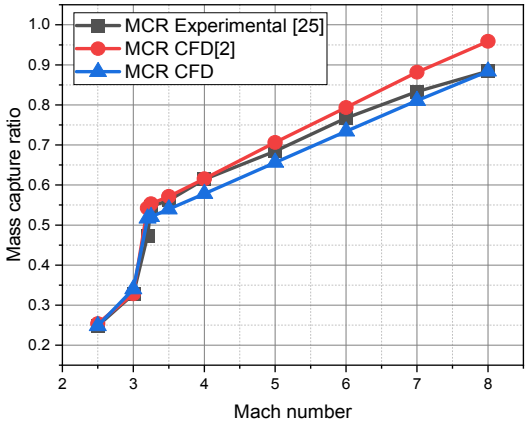

Figure 8. Comparison of mass capture ratio for different free-stream Mach numbers

This demonstrates the significance of the oblique shock wave caused by the first ramp. The first oblique shock must be attached to the cowl to achieve the highest MCR. The maximum MCR value was obtained at Mach 8, closely corresponding to experimental data [25].

TPR given in figure 9 also shows quite a good agreement between the reference data [2, 25] and the present 2D simulation.

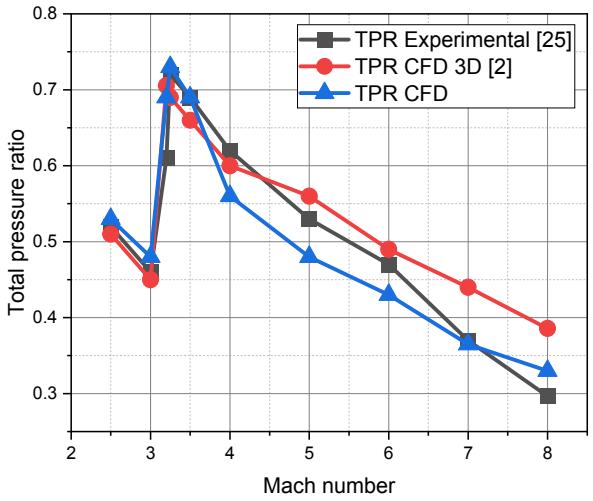

Figure 9. Comparison of total pressure ratio for different free-stream Mach numbers

Hence, from figure 7,8,9 we can say that the in-house algorithm adopted to solve the supersonic and hypersonic case has well captured the flow physics.

5. RESULTS AND DISCUSSION

5.1 Air-intake start & unstart issues with bleed

The throat of the Air-intake must be inside the geo–metry, and the normal shock must be present just downstream of the throat for the starting condition. The contraction ratio is a critical parameter that effectively controls the starting behavior of an intake [31]. A low contraction ratio increases the chance of starting as the flight Mach number increases. However, this leads to a large area of the throat that may degrade the intake performance. Due to the flow spillage during the unstart condition, the spillage drag of the intake increases. The main reason for the intake unstart for the Hypersonic inlet is the boundary layer separation caused by the shock wave-boundary layer interaction at the intake entrance. Bleed has the capability to solve both the supersonic and the hypersonic unstart problem, and the bleed increases the actual flow area at the throat, which improves the amount of the intake mass flow.

5.2 Simulation for different free-stream Mach number

The starting and unstarting criteria of intake affect the overall engine performance, so analysing the intake with different free-stream Mach numbers is necessary. To determine the start and unstart conditions of the inlet, simulations were run for the supersonic and the hypersonic Mach numbers. The converged solution, corresponds to a higher Mach number, is fed as the initial flow field values. The simulation is carried out with free-stream Mach values of 2.5, 3, 3.2, 3.3, 3.5, 4, 5, 6, 7, and 8.

Figures 8 and 9 depict the variation in TPR for various free-stream Mach numbers without bleed. The total pressure ratio (TPR) is the ratio of the total pressure at the outlet to the total pressure at the inlet. For the optimal inlet performance, TPR and MCR both should be at their optimal condition. Here we can see that the TPR (fig 9) drops from the Mach number 2.5 to 3 and then reaches its peak near the Mach number range of 3.2-3.3. But if we look at Figure 8, we can see that MCR rises from 2.5 to 3, and then a sharp rise in MCR occurs near Mach 3-3.3. So, a critical point occurs near Mach 3-3.3. After this limit, TPR starts falling down and MCR further shoots up, and the pattern formed by them is quite smooth without much change in trend. So, understanding the flow physics at this particular Mach number is quite significant. Therefore, for this research we have undertaken a detailed effect of Bleeding only after Mach 3. The graph shows a sudden drop in TPR around Mach 3 due to shockwave boundary layer interaction, indicating the inlet unstart.

5.3 flow physics and effect of bleed size on TPR and MCR

Development of critical intake conditions near the mach 3 has been captured by analyzing multiple cases at Mach 3, 3.2, 3.3, and 3.5. The Mach number distri–bution for the free-stream Mach number 3.2 is shown in Figure 10. The figure also includes an enlarged view. The interaction of Mach 3.3 with the first ramp pro–duces a weak oblique shock that is not attached to the cowl and originates above it, indicating spillage. The reflected shock interacts with the lower ramp once more, causing the boundary layer to interact with the shockwave, resulting in poor performance. In addition, the cowl shock is repeatedly reflected by both the ramp and the top wall, resulting in a train of oblique shocks inside the intake that compresses the flow even more.

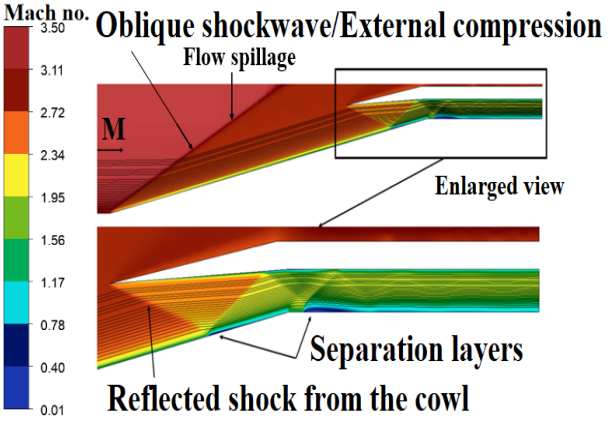

Figure 10. Mach number contour for M=3.3

The zone of the separation bubble is also shown in the form of a velocity streamline plot in Figure 11 and a velocity vector in Figure 12. After this first separation bubble, some more separation bubbles are also visible, but it diminishes gradually along the length, as shown in Figure 12.

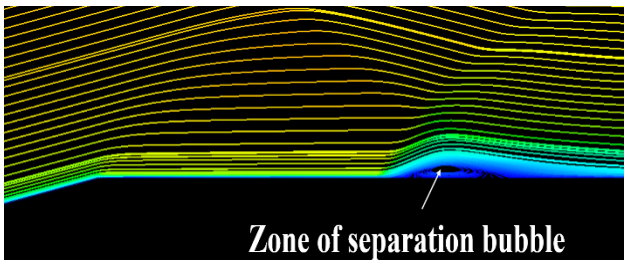

Figure 11. Velocity streamline plot inside the intake

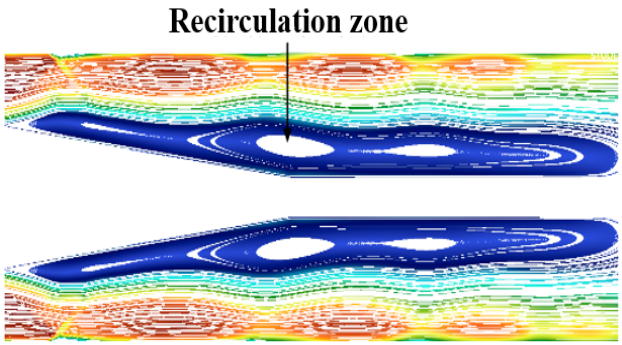

Fig 12. Velocity vector showing recirculation eddies

Figure 13 to 16 shows the Mach contours with a superimposed streamline for a different bleed section of 1.6 mm, 3 mm, 7.1 mm, and 8.6 mm, respectively, at M=3.3.

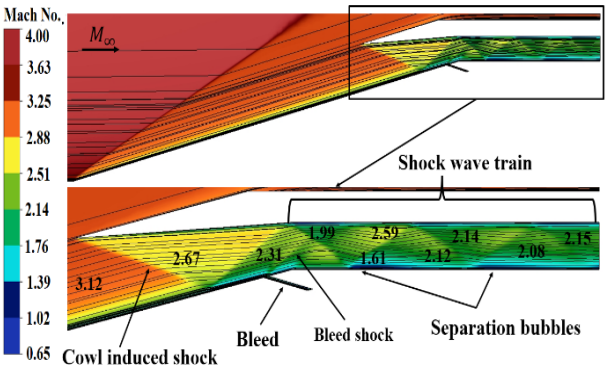

Figure 13. Instantaneous Mach number contour for bleed section 1.6mm at M=3.3

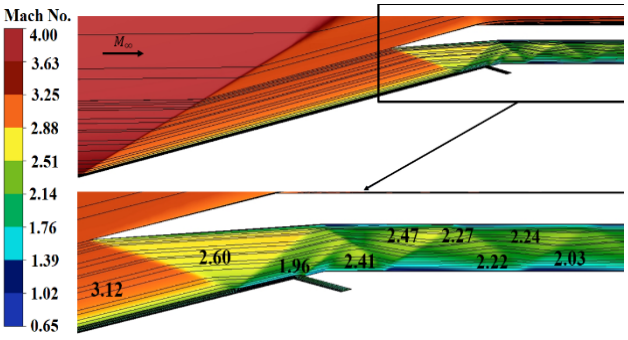

Figure 14. Instantaneous Mach number contour for bleed section 3mm at M=3.3

As per Figure 17, the TPR for almost all bleed geometry is almost the same at or near Mach 3-4, but their effect becomes prominent as we increase the ope–rating Mach number. TPR for 1.6mm bleed is almost the same as for no bleed configuration. TPR keeps on increasing with increased bleed size. At Mach 6, TPR for 8.6mm bleed is the highest. The shockwave is also modified near the bleed, as shown in Figure 13-16. Separation bubbles exist after the bleeding in all cases. The 3 mm and 7.1 mm bleed sections exhibit the same trend until Mach 6. At around Mach 8, the TPR of bleed size 7.1mm almost coincides with TPR without bleed, and the bleed size of 3mm coincides with the bleed size of 8.6mm. The 8.6mm bleed indicates that it provides the best TPR while operating between Mach 4 and 6; it provides almost 20% increase in TPR over no-bleed configurations but gradually decreases for Mach 8, where the increase in TPR over no bleed is around 15%. 3mm bleed consistently shows a linear pattern throughout the Mach number range of 4 to 8. The bleed has a consistently higher TPR of around 15%.

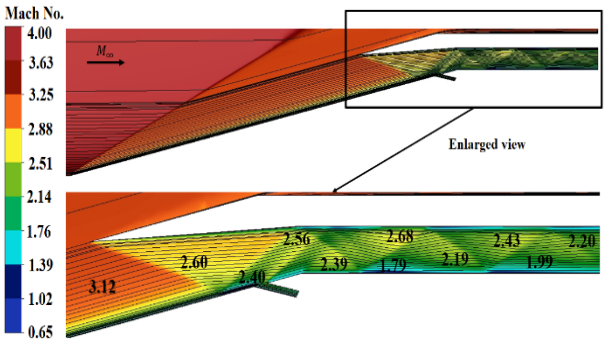

Figure 15. Instantaneous Mach number contour for bleed section 7.1mm at M=3.3

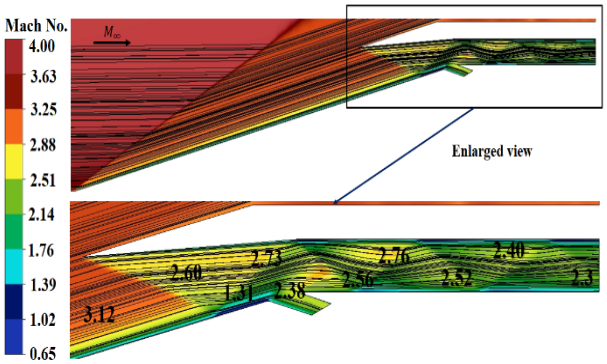

Figure 16. Instantaneous Mach number contour for bleed section 8.6mm at M=3.3

The impact of the MCR is almost similar to that of TPR. However, the overall mass flow rate of the air-intake system is a significant factor, and it has been provided in Tables 2-5.

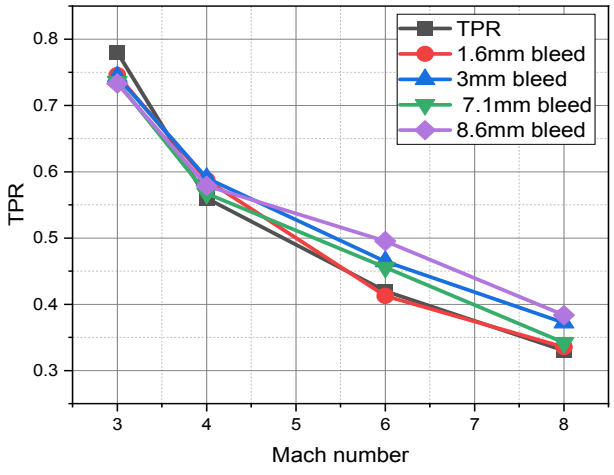

Figure 17 Bleed effect on total pressure ratio

Table 2 and 5 below shows the percentage drop in the mass flow rate when different bleed geometries are implemented in the air-intake model.

Table 2. Percentage drop in mass flow rate in the air-intake at bleed size= 1.6175mm

Sl. No.	Mach no.	% drop in MFR (appx)
1	3	1.53955
2	4	1.314169
3	6	0.6138
4	8	0.77629

Table 3. Percentage drop in mass flow rate in the air-intake at bleed size= 3 mm

Sl. No.	Mach no.	% loss in MFR (appx)
1	3	0.175241
2	4	2.936982
3	6	2.018282
4	8	0.057107

Table 4. Percentage drop in mass flow rate in the air-intake at bleed size= 7.131mm

Sl. No.	Mach no.	% drop in MFR (appx)
1	3	3.352975
2	4	3.893315
3	6	1.597731
4	8	0

Table 5. Percentage drop in mass flow rate in the air-intake at bleed size= 8.6 mm

Sl. No.	Mach no.	% drop in MFR (appx)
1	3	8.507176
2	4	3.893315
3	6	9.310046
4	8	5.0122798

As per the table, if we compare the percentage drop in MFR for the bleed size of 3mm and 8.6mm, we can see the loss is significant in the latter. As we know, the thrust generated by the engine is a function of MFR, so there will be a huge thrust loss in the 8.6mm bleed compared to the 3mm bleed, making it unfit for implementation. On the contrary, the TPR of 3mm and 8.6mm are in close agreement.

6. CONCLUSION

Air intake is an essential part of a high-speed engine, and its design impacts the engine's overall performance. Computational studies of the 2D supersonic and hypersonic air intake with and without bleed are presented in this paper. In-house algorithm and code are fed on commercial CFD software, coupled with density-based RANS equations, and further solved with a k-ωSST turbulence model. The computed wall pressure distribution and intake performance parameters (TPR and MCR) reasonably match the experimental results. The steady-state simulations were performed for various free-stream Mach numbers ranging from 2.5 to 8. The sudden drop in the mass capture and total pressure ratio determines the free-stream Mach number at which intake unstarting occurs. The bleed geometry in this paper has been shown to delay the flow separation that reduces the contraction ratio, hence, the effective throat area. It also increases engine performance through increased TPR. Sincethe bleed geometry also reduces the mass flow rate, in the current paper, we have also tried to maintain the trade-off between the MFR and TPR. The air intake has been studied with four different bleed sections ranging in size from 1.6mm to 8.6mm. Critical Mach number where the abrupt transition in the value of TPR and MCR occurs is obtained in the range of 3-3.3.

Further simulations with bleed geometry were run from Mach numbers 3 to 8. Low Mach number like 3-3.3 hardly shows any improvement with the bleed, but their effect becomes more dominant when we cross Mach number 4. Among different bleed geometries, the 3mm bleed diameter is the most consistent among its peers as its performance remains almost constant from Mach 4 to 8. In Tables 2-5, we can see that as the size of the bleed increases, the drop in MFR also increases. 8.6mm bleed geometry has undoubtedly increased the TPR over the non-bleed geometry, but it's only for a small range of Mach 4-6 at the cost of thrust loss. At Mach 8, the TPR improvement achieved with 3mm and 8.6mm bleed is almost the same. Taking into account the loss in the mass flow rate due to the 8.6mm bleed, we recommend that a 3mm bleed is an ideal trade-off while operating at different Mach numbers of 4-8.

The unsteady analysis will provide the amplitude and frequency of the buzz phenomena for the same set of bleed geometries. It will be the scope of further research.

ACKNOWLEDGMENT

The authors would like to thank the Amity Institute of Aerospace Engineering faculty and staff members, who provided valuable feedback during this research.

REFERENCES

[1] Saha, S., Chakraborty, D.: Role of viscosity in hypersonic intake starting phenomenon, Journal of Aerospace Sciences & Technologies, Vol. 69, No. 1, 2017.

[2] Saha, S. and Chakraborty, D.: Hypersonic Intake Starting Characteristics–A CFD Validation Study. Defence Science Journal, Vol. 62, pp.147-152.

[3] Ogura, S. et al: Experimental study of high-speed air intake performance by side clearance, Aerospace Science and Technology, Vol. 123, April 2022.

[4] Soltani M., Sepahi Younsi J. and Daliri A.: Performance investigation of a supersonic air intake in the presence of the boundary layer suction. Proceedings of the Institution of Mechanical Engineers, Part G: Journal of Aerospace Engineering, Vol. 229, No.8, pp. 1495-1509, 2015

[5] James, J.K. and Kim, H.D.: Flow Characteristics of a Mixed Compression Hypersonic Intake, Journal of Applied Fluid Mechanics, Vol. 15, No. 3, pp. 633-644, 2022.

[6] Liu, X., Shi, L., Liu, P., Qin, F.and He, G.: Design and Numerical Investigations on a Dual-Duct Variable Geometry RBCC Inlet, International Journal of Turbo & Jet-Engines, Vol. 37, Issue 2, 2020

[7] Chang et al.: Recent research progress on unstart mechanism, detection, and control of hypersonic inlet, Progress in Aerospace Sciences, Vol. 89, pp. 1-22, February 2017,

[8] Ebrahimi, A., Chavoshi, M.Z.: Numerical Inves–tigation of Back Pressure and Free-stream Effects on a Mixed Compression Inlet Performance, Scientia Iranica, Transactions B, Mechanical Engineering, Vol.25, pp. 751-761, 2018

[9] Tanguy, G. and Macmanus, D.G.: Characteristics of Unsteady Total Pressure Distortion for a Complex Aero-engine Intake Duct, Aerospace Science and Technology, Volume 78, July 2018, Pages 297-311.

[10] Sun, Z., Gan, T., Wu, Y.: Shockwave/ Boundary-Layer Interactions at Compression Ramps Studied by High-Speed Schlieren, AIAA Journal, Vol. 58, No. 4, 2020.

[11] Huang, W., Wu, H., Yang, Y., Yan, L. and Liu, S.: Recent advances in the shock wave/boundary layer interaction and its control in internal and external flows, Acta Astronautica, Vol. 174, pp. 103-122, 2020.

[12] Hebrale, J. and Gulhan, A.: Internal flow field investigation of hypersonic inlet at Mach 6 with bleed. J. Propulsion Power, Vol. 23, No.5, pp. 1007-017,2007

[13] Im, Seong-Kyun, and Do, H.: Unstart phenomena induced by flow choking in scramjet inlet-isolators. Progress in Aerospace Sciences, Vol. 97, pp. 1-21, 2018.

[14] Reinartz, B.U, Herrmann, C.D., Ballmann, J. and Koschel, W.W.: Aerodynamic Performance Analysis of a Hypersonic Inlet Isolator Using Computation and Experiment, J. of propulsion and power, Vol. 19, No. 5, 2003.

[15] Schmitz, D.M. and Bissinger, N.C: Design and testing of 2-D mixed –Geometry hypersonic intakes, AIAA Paper No. 98-1529, 1998.

[16] Wang, Y., Wang, Z., Liang, J. And Fan., X.: Investigation on Hypersonic Inlet Starting Process in Continuous Free jet Wind Tunnel, Journal of propulsion and power, Vol. 19, No. 5, 2003.

[17] Reinartz, B. and Behr, M.: Influence of Sidewall Compression on Hypersonic Intake Performance,16th AIAA/DLR/DGLR International Space Planes and Hypersonic Systems and Technologies Conference, October 2009.

[18] Sekar, K.R. Karthick, S.K., Jegadheeswaran, S. and Kannan, R.: On the unsteady throttling dynamics and scaling analysis in a typical hypersonic inlet-isolator flow, Physics of Fluids, Vol. 32, Issue 12, 2022.

[19] Lee, C. and Chen, S.: Recent progress in the study of transition in the hypersonic boundary layer. Natl Sci Rev. Vol. 6, No.1, pp.155-170. 2019

[20] Kumar, G. and De, A.: Modes of unsteadiness in shock wave and separation region interaction in hypersonic flow over a double wedge geometry, Physics of Fluids, Vol. 33, Article No. 076107 2021

[21] Janarthanam, S. and Babu, V.: Numerical simulations of the flow through the inlet and isolator of a Mach 4 dual-mode scramjet, The Aeronautical Journal, Vol. 116, No. 1182, pp. 833-846, 2012.

[22] Yates, H.B., Matlis, E.H., Juliano, T.J. and Tufts, M.W.: Plasma-Actuated Flow Control of Hypersonic Cross flow-Induced Boundary-Layer Transition, AIAA Journal, Vol. 58, No.5, 2020.

[23] Wartemann, V., Wagner, A., Kuhn, K., Eggers, T. and Hannemann, K.: Passive Hypersonic Boundary Layer Transition Control Using an Ultrasonically Absorptive Coating With Random Microstructure: Computational Analysis Based on the Ultrasonic Absorption Properties of Carbon-Carbon, Procedia IUTAM, Vol 14, pp. 413-422, 2015.

[24] Barber, T.J., Hiett, D. and Fastenberg, S.: CFD modelling of the hypersonic inlet starting problem. AIAA Paper No. 2006-0123, 2006.

[25] Emami, S. and Trexler, C.: A. Experimental investigation of inlet combustor – isolators for a dual mode scramjet at a Mach number of 4. NASA Technical Report No. NASA TP3502, May 1995.

[26] Sanal Kumar, V.R., Sankar, V., Nichith, C., Saravanan, V., et al.: A closed-form analytical model for predicting 3D boundary layer displacement thickness for the validation of viscous flow solvers, AIP Advances, Vol. 8, Issue: 02, Article No. 025315, 2018.

[27] Sanal Kumar, V.R., et al.: Diagnostic Investigation of Stream tube Flow Choking Effects on the Aerodynamic Performance of Transonic Aircraft, AIAA 2022-1955.

[28] Milićev, S.S.: An Experimental Study of the Influence of Spike in Supersonic and Transonic Flows Past a Hemispheric Body, FME Transactions, Vol. 50, No. 1, PP. pp. 24-31, 2022.

[29] Damljanović, D., Vuković, D., Ocokoljić, G. and Rašuo, B.: Convergence of Transonic Wind Tunnel Test Results of the AGARD-B Standard Model, FME Transactions, Vol. 48, No. 4, pp. 761-769, 2020.

[30] Damljanović, D., Vuković, Đ., Ocokoljić, G., Ilić B., and Rašuo, B.: Wind Tunnel Testing of ONERAM, AGARD-B and HB-2 Standard Models at Off-Design Conditions, Aerospace, Vol. 8, No. 10, 275, 22 Sep. 2021.

[31] Sepahi-Younsi J, Forouzi Feshalami B, Maadi S, R. and Soltani M, R.: Boundary layer suction for high-speed air intakes: A review. Proceedings of the Institution of Mechanical Engineers, Part G: Journal of Aerospace Engineering, Vol. 233, No. 9, pp. 3459-3481, 2019.

NOMENCLATURE

2D RANS	Two-Dimensional Reynolds-averaged Navier–Stokes
k - ωSST	k – ω shear stress transport model
k	Turbulent kinetic energy
ω	Specific dissipation rate

ρ	Density
x_i, x_j	Spatial coordinates
α	the coefficient that depends on the spe–cific implementation of the turbulence model
u_i, u_j	Velocity tensor
G_k	It represents the generation of turbulent kinetic energy due to mean velocity gradients
ε	Turbulence dissipation rate
μ	Dynamic viscosity
μ_t	Turbulent viscosity
Pr_k	Turbulent Prandtl number for turbulent kinetic energy
Pr_ω	Turbulent Prandtl number for the specific dissipation rate
Pr_γ	Turbulent Prandtl number for thermal conductivity
β*	A constant coefficient
τ_{ij}	Stress tensor
γ	Thermal conductivity of the fluid
γ_t	turbulent thermal conductivity
T	Temperature
T_{ref}	Reference temperature specified (273K)
μ_{ref}	Dynamic viscosity of the fluid at T_{ref}
S	Sutherland constant
Q	Heat source or sink terms
E	Total Energy per unit mass
c_μ	Turbulent viscosity constant
PDE	Partial Differential equation
P	Pressure
P_{inf}	Free stream pressure
TPR	Total pressure ratio
MCR	Mass capture ratio
MFR	Mass flow rate
CFD	Computational Fluid dynamics
M/M_∞	Mach number/Free stream Mach number
L	Length of the upstream symmetry section
x/h	The ratio of wetted length and the intake throat height

ПАСИВНА МОДИФИКАЦИЈА ПРОТОКА ПРЕКО СУПЕРСОНИЧНОГ И ХИПЕРСОНИЧНОГ СИСТЕМА ЗА УСИСАВАЊЕ ВАЗДУХА ПОМОЋУ ОДВОДА

Ц. Сина, С. Синг, О. Пракаш, Д. Панчал

Усисник ваздуха треба да ради у пројектованим условима да би се постигао висок укупни опоравак притиска и оптималан однос масе. Актуелно истра–живање се фокусира на нумеричку симулацију надзвучног и хиперсоничног улаза ваздуха и њего–вих почетних и непокренутих карактеристика. 2D RANS једначина за суперсонични и хиперсонични унос је решена коришћењем k-ωSST модела турбу–ленције. Ин-хоусе код и алгоритам заснован на RANS једначини су такође валидирани у одговарајућем поступку и коришћени за накнадне симулације. Нагли пад у односу масе указује на непо–кренуто стање уноса. Присуство одводног дела има похвалан ефекат на параметар перформанси усисника ваздуха. Уочен је мехур одвајања на улазу у усис током ванпројектованих услова, што је резултирало губицима перформанси. Коришћена су четири различита одељка за испуштање у распону величине од 1,6 мм до 8,6 мм, а симулације са блидом су вођене за различите Махове бројеве у распону од 3 до 8. Оптимална величина испуштања од 3 мм се показала прилично ефикасном у модификацији укуп–ног опоравка притиска унутар оптимални масени проток у широком опсегу Махових бројева.